



# Unusual Emission Variations Near the Eclipse of Black Widow Pulsar PSR J1720–0533

S. Q. Wang<sup>1,2,3,4</sup>, J. B. Wang<sup>1,3,4</sup>, N. Wang<sup>1,3,4</sup>, J. M. Yao<sup>1,3,4</sup>, G. Hobbs<sup>5</sup>, S. Dai<sup>6</sup>, F. F. Kou<sup>1,3,4</sup>, C. C. Miao<sup>7</sup>, D. Li<sup>7,8</sup>, Y. Feng<sup>9</sup>, S. J. Dang<sup>10</sup>, D. H. Wang<sup>10</sup>, P. Wang<sup>7</sup>, J. P. Yuan<sup>1,3,4</sup>, C. M. Zhang<sup>7</sup>, L. Zhang<sup>7</sup>, S. B. Zhang<sup>11</sup>, and W. W. Zhu<sup>7</sup>

<sup>1</sup>Xinjiang Astronomical Observatory, Chinese Academy of Sciences, Urumqi, Xinjiang 830011, People's Republic of China; [wangjingbo@xao.ac.cn](mailto:wangjingbo@xao.ac.cn), [na.wang@xao.ac.cn](mailto:na.wang@xao.ac.cn)

<sup>2</sup>CAS Key Laboratory of FAST, NAOC, Chinese Academy of Sciences, Beijing 100101, People's Republic of China

<sup>3</sup>Key Laboratory of Radio Astronomy, Chinese Academy of Sciences, Urumqi, Xinjiang, 830011, People's Republic of China

<sup>4</sup>Xinjiang Key Laboratory of Radio Astrophysics, Urumqi, Xinjiang 830011, People's Republic of China

<sup>5</sup>CSIRO Astronomy and Space Science, PO Box 76, Epping, NSW 1710, Australia

<sup>6</sup>School of Science, Western Sydney University, Locked Bag 1797, Penrith South DC, NSW 2751, Australia

<sup>7</sup>National Astronomical Observatories, Chinese Academy of Sciences, Beijing 100101, People's Republic of China

<sup>8</sup>NAOC-UKZN Computational Astrophysics Centre, University of KwaZulu-Natal, Durban 4000, South Africa

<sup>9</sup>Zhejiang Lab, Hangzhou, Zhejiang 311121, People's Republic of China

<sup>10</sup>School of Physics and Electronic Science, Guizhou Normal University, Guiyang 550001, People's Republic of China

<sup>11</sup>Purple Mountain Observatory, Chinese Academy of Sciences, Nanjing 210008, People's Republic of China

Received 2021 August 19; revised 2021 November 2; accepted 2021 November 4; published 2021 November 18

## Abstract

We report on an unusually bright observation of PSR J1720–0533 using the Five-hundred-meter Aperture Spherical radio Telescope (FAST). The pulsar is in a black widow system that was discovered by the Commensal Radio Astronomy FAST Survey (CRAFTS). By coincidence, a bright scintillation maximum was simultaneous with the eclipse in our observation, which allowed for precise measurements of flux density variations, as well as dispersion measure (DM) and polarization. We found that there are quasi-periodic pulse emission variations with a modulation period of  $\sim 22$  s during the ingress of the eclipse, which could be caused by plasma lensing. No such periodic modulation was found during the egress of the eclipse. The linear polarization of the pulsar disappears before the eclipse, even before there is a visually obvious change in DM. We also found that the pulse scattering may play an important role in the eclipse of PSR J1720–0533.

*Unified Astronomy Thesaurus concepts:* [Radio pulsars \(1353\)](#); [Millisecond pulsars \(1062\)](#); [Eclipsing binary stars \(444\)](#)

## 1. Introduction

Redbacks (RBs) and black widows (BWs), jointly known as the spider pulsars, are an interesting subset of the pulsar population (Roberts 2013; Patruno et al. 2017). Spider pulsar systems comprise a millisecond pulsar (MSP) with a low-mass companion in short, near-circular orbits. The two types are distinguished by the masses of their companions, with RB companion masses  $\sim 0.2$ – $0.4 M_{\odot}$ , and BW companion masses  $\sim 0.01$ – $0.05 M_{\odot}$  (Roberts 2013). Most of known spider systems show periodic eclipses of the radio emission centered approximately around the inferior conjunction of the companions. The eclipses happen when the radio emission is blocked by the companions or outflowing material. The presence of material beyond the Roche lobes and strong irradiation indicate the companion will be ablated by the emission from the neutron star (Fruchter et al. 1988).

The eclipses of spider pulsars are frequency dependent, usually with longer duration at lower frequency, and sometimes no eclipses are seen at all at high frequency (Stappers et al. 2001; Polzin et al. 2018, 2019). Although many eclipse mechanisms have been proposed, there is no apparent consensus on the correct eclipse mechanism. Different mechanisms may be responsible for the eclipses in different systems (Thompson et al. 1994). Magnetic fields in the eclipse

medium are required for some of the promising mechanisms. The presence of a magnetic field of the eclipse material is suggested by the linear depolarization near the eclipse for the RB PSR J1748–2446A (You et al. 2018). Crowter et al. (2020) measured a nonzero magnetic field in the eclipse material of the BW PSR J2256–1024.

Spider pulsars are considered to be descendants of low-mass X-ray binaries (LMXBs) after accretion onto the pulsar has terminated (Bhattacharya & van den Heuvel 1991). Systems with transitions between LMXBs and radio pulsars have been seen in three RBs (e.g., Archibald et al. 2009; Stappers et al. 2014), which have strongly inspired the typical MSP recycling theory (Alpar et al. 1982). The ablation of a companion after accretion may lead to complete destruction of the companion star, contributing to the observed isolated MSPs (Fruchter et al. 1988). Apart from evolutionary studies, spider pulsars could also offer valuable opportunities to investigate the pulsar wind and characteristics of the companion stars under intense irradiation.

Plasma lensing was detected surrounding eclipses in three spider pulsars in the past few years, BW PSR B1957+20 (Main et al. 2018), RB PSR B1744–24A (Bilous et al. 2019), and BW PSR 2051–0827 (Lin et al. 2021). The effects of plasma lensing were seen as highly magnified pulses. The plasma lensing was used to resolve the pulse emission, constraining emission sizes and separations. Main et al. (2018) inferred a resolution of the plasma lensing of PSR B1957+20 of about 10 km, which is comparable to the pulsar's radius. However, this method is limited by understanding and modeling of the lenses.



Original content from this work may be used under the terms of the [Creative Commons Attribution 4.0 licence](#). Any further distribution of this work must maintain attribution to the author(s) and the title of the work, journal citation and DOI.

The radio emissions of the spider pulsars are generally weak near the eclipses. Highly sensitive radio telescopes such as the Five-hundred-meter Aperture Spherical radio Telescope (FAST) provides a great opportunity to study the eclipse in detail. PSR J1720–0533 is a pulsar in the Galactic field that was newly discovered by the Commensal Radio Astronomy FAST Survey (CRAFTS; see Li et al. 2018) and was confirmed to be a BW by a FAST key science project: pulsar physics and evolution (project id: ZD2020\_6) with a 3.26 ms spin period, a 3.16 hr orbital period, and a  $\sim 0.034 M_{\odot}$  companion. The dispersion measure (DM) is  $36.8337 \pm 0.0006 \text{ cm}^{-3} \text{ pc}$  with the DM-derived distance of 191 pc using the electron density model of Yao et al. (2017). The timing solution for the pulsar will be presented by C. C. Miao et al. (2021, in preparation). In the Letter, we present the unusual emission variations near the eclipse of PSR J1720–0533 using FAST. In Section 2, we describe our observation and data processing. In Section 3, we present the results. We discuss and summarize our results in Section 4.

## 2. Observations and Data Processing

FAST is located in Guizhou, China, with its whole aperture of 500 m and an illuminated subaperture of 300 m during normal operation. A 19-beam receiver covering 1.05–1.45 GHz provides two data streams (one for each linear polarization; Jiang et al. 2019). The observation was carried out using the central beam of the 19-beam receiver on 2020 August 25. The data were captured by a digital backend based on Reconfigurable Open-architecture Computing Hardware version 2 (ROACH2) and recorded in search mode PSRFITS format with four polarizations, 8-bit, 49.152  $\mu\text{s}$  sampling interval, and 4096 frequency channels, respectively. A total of 7139 s of observations were recorded.

The data were processed to remove dispersion delay caused by the interstellar medium and folded modulo the predicted pulse period and integrated every 1 s using DSPSR (van Straten & Bailes 2011). PSRCHIVE programs PAZ and PAZI (Hotan et al. 2004) were used to flag and remove narrowband and impulsive radio-frequency interference (RFI) of the data. A polarization calibration noise signal was injected and recorded after the pulsar observation. Polarization calibration was achieved by correcting for the differential gain and phase between the receptors through separate measurements using the noise diode signal. Flux density was calibrated using observations of 3C 286. Rotation measure (RM) was measured using the PSRCHIVE program RMFIT (Hotan et al. 2004). The dispersion measure (DM) for each subintegration was measured using the TEMPO2 software package (Hobbs et al. 2006). More detail on obtaining DM is given in Section 3.3.

## 3. Results

### 3.1. Emission Variations Near the Eclipse

The averaged pulse emissions of PSR J1720–0533 with subintegrations of 1 s are shown in the upper panel of Figure 1. The pulse intensity becomes weaker, variable dispersion is seen through the shift of the pulse profile, and the profile is visibly scattered at the eclipse boundary. The pulsar underwent a strong scintillation that began around an orbital phase of 0, which strengthened the emissions during the eclipse. Note that this is interstellar scintillation, which is unrelated to the eclipse or eclipsing material. To measure the eclipse duration, a Fermi–

Dirac function was used to fit the pulse flux density variations during the ingress and egress. More detail on the fitting is shown in Section 3.2. The flux density was measured using the PSRCHIVE software package. The eclipse duration was taken as the width of the eclipse at half-maximum of the flux density. The eclipse lasts about  $1495 \pm 2 \text{ s}$ , which accounts for about 13.14% of the orbital period. A mini-eclipse is seen at the orbit phase of 0.37 (the red square in the upper panel of Figure 1) with a duration of approximately dozens of seconds. The mini-eclipses generally occur at different orbit phases in spider pulsars, which were attributed to clumps of plasma surrounding the eclipse medium (Deneva et al. 2016; Polzin et al. 2019).

Enlargements of the ingress and egress of the eclipse are shown in the middle panels of Figure 1. We found that the pulse emission of the pulsar during the ingress shows significant modulations and there are six bright emission clusters that are labeled as “I,” “II,” “III,” “IV,” “V,” and “VI,” respectively (see the middle left panel of Figure 1). No such periodical modulations are detected during the egress of the eclipse (see the middle right panel of Figure 1). The flux densities during the ingress and egress gradually decreased and increased, respectively. The duration of the ingress lasts longer than the egress and therefore the eclipse of PSR J1720–0533 is asymmetric. The asymmetry eclipse of spider pulsars may be due to a cometary-like tail of the intrabinary material that results from the orbital motion of the companion (Fruchter et al. 1988; Main et al. 2018). The tail generally leads to eclipse egress lasting substantially longer than ingress (Tavani & Brookshaw 1991).

The dynamic spectra during the ingress of PSR J1720–0533 are shown in the upper panel of Figure 2. These six bright emission clusters are also clearly seen in the dynamic spectra, and they are unrelated to the interstellar scintillation. Similar phenomena have also been seen in the BW PSR J2051–0827, which may result from plasma lensing by the companion’s material (Lin et al. 2021). The plasma lensing possibly occurs during the eclipse ingress of PSR J1720–0533 as well. We then investigated the periodicity of the modulations during the ingress of the eclipse. We subtracted the Fermi–Dirac fitting results from the flux density during the ingress and then calculated the autocorrelation function (the bottom panel of Figure 2). We found that the correlation coefficient reaches its maximum at a time lag of 22 s, which suggests that the modulations during the ingress of eclipse are quasi-periodic with a period of  $\sim 22 \text{ s}$ . The Fermi–Dirac fits are used to estimate the average magnification of lensing, and we obtained that the magnification is in the range of about 0.4–1.6 during the eclipse ingress.

### 3.2. Frequency-dependent Eclipse

To investigate the frequency dependence of the eclipse, we divided the entire band into four equal subbands with the central frequencies of 1100 MHz, 1200 MHz, 1300 MHz, and 1400 MHz, respectively (Figure 3). The duration of the eclipse was taken as the FWHM of the flux density and was calculated by fitting the ingress and egress flux densities with Fermi–Dirac functions  $f = A \left( e^{\frac{\phi - P_1}{P_2}} + 1 \right)^{-1}$  with the amplitude  $A$ , the time at half-maximum of the pulse flux density  $P_1$ , and the slope  $P_2$ , which was used to fit the flux density variations for the eclipse at each subband (Polzin et al. 2018). The eclipse durations at these four subbands are  $1513 \pm 3 \text{ s}$ ,  $1517 \pm 7 \text{ s}$ ,  $1483 \pm 3 \text{ s}$ , and

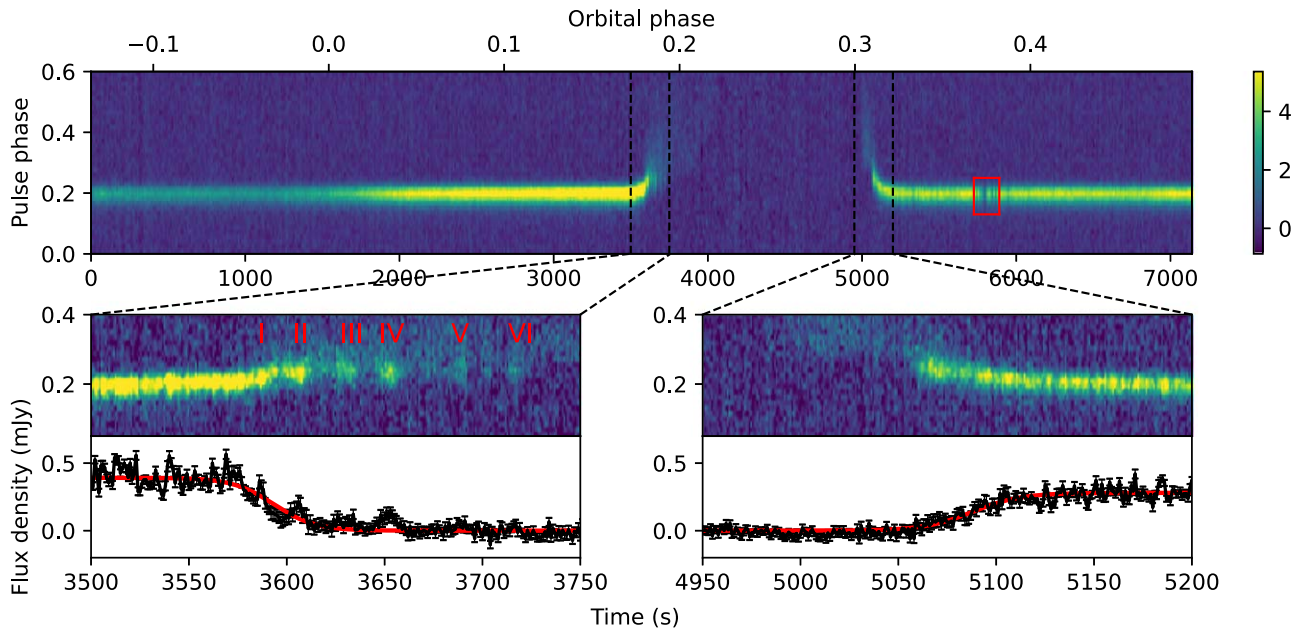


**Figure 1.** The upper panel shows the total intensity of pulse emission versus pulsar spin and orbital phases with a subintegration of 1 s of PSR J1720–0533. A mini-eclipse is labeled with the red box. Enlargements of the ingress and egress of the pulsar are shown in the middle left and middle right panels, respectively. In the middle left panel, these six bright clusters are labeled as “I,” “II,” “III,” “IV,” “V,” and “VI,” respectively. The bottom panels show the pulse flux density variations near the eclipse. The red curves show least-squares fit of Fermi–Dirac functions to the ingress and egress of the eclipse.

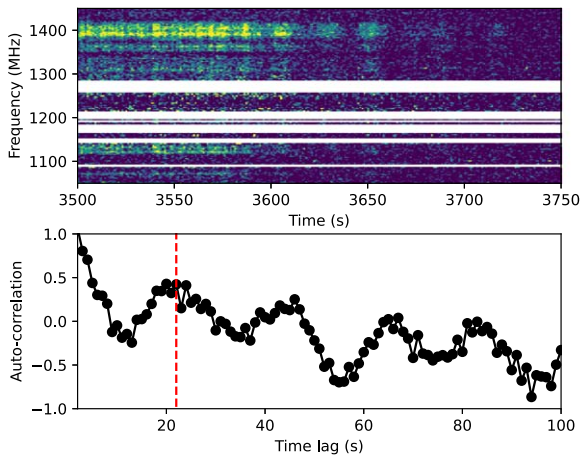


**Figure 2.** Upper panel: the dynamic spectrum during the ingress of PSR J1720–0533. Note that the frequency was binned into 256 channels and some channels are zapped because of RFI. Bottom panel: the autocorrelation function for the difference between the pulse flux density and the Fermi–Dirac fitting results during the ingress of the eclipse. The red dashed line is for the lag of 22 s with a Pearson correlation coefficient of about 0.42.

$1472 \pm 2$  s, respectively. Like other spider pulsars, the eclipse of PSR J1720–0533 lasts longer at lower frequencies. However, the eclipse duration is not monotonically decreasing with increasing frequency because of the effect of scintillation that makes it is hard to confirm where the eclipse begins or ends. Our results are limited by the observational frequency bandwidth and observations with an ultrawide-band receiver will provide more information on the eclipse. We used a power-law function to fit the eclipse duration variations with increasing frequency and obtained that the index  $\alpha = -0.14 \pm 0.07$ , which is flatter than that of PSR B1957 +20 at  $-0.41 \pm 0.09$  (Fruchter et al. 1988) or PSR J1810 +1744 at  $-0.41 \pm 0.03$  (Polzin et al. 2018). Power-law functions were also used to fit both ingress and egress

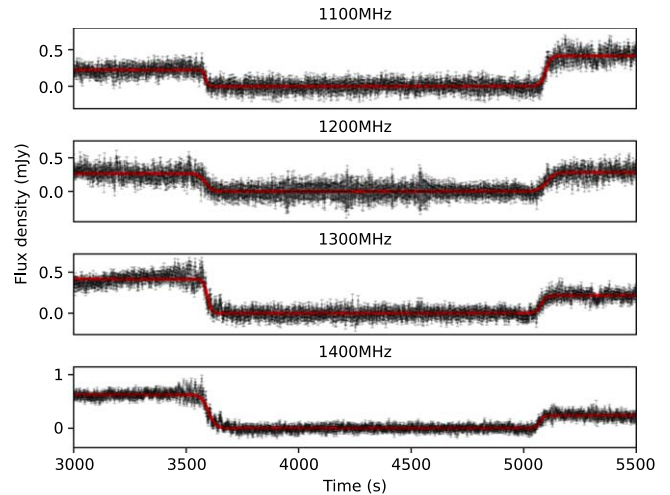


**Figure 3.** Flux density variations for the eclipse of PSR J1720–0533 at different frequencies. The red line shows the least-squares fit of the Fermi–Dirac function to the ingress and egress at each frequency subband.

durations, and we obtained that the indices for ingress and egress are  $-0.07 \pm 0.02$  and  $-0.18 \pm 0.07$ , respectively. The duration of egress is more frequency dependent than that of ingress.

### 3.3. DM and Polarization Profile Variations

TEMPO2 software packages (Hobbs et al. 2006) were used to obtain the DM during the eclipse. The data are folded with a subintegration of 30 s. Then, we crunched our data to four frequency channels with a bandwidth of 100 MHz. A noise-free template was formed by fitting the integrated profile of the entire out-of-eclipse observation and pulse times of arrival (ToAs) were formed by cross-correlating pulse profiles with the standard template. We fitted the DM of each subintegration during the ingress and egress of of the pulsar, and the DM

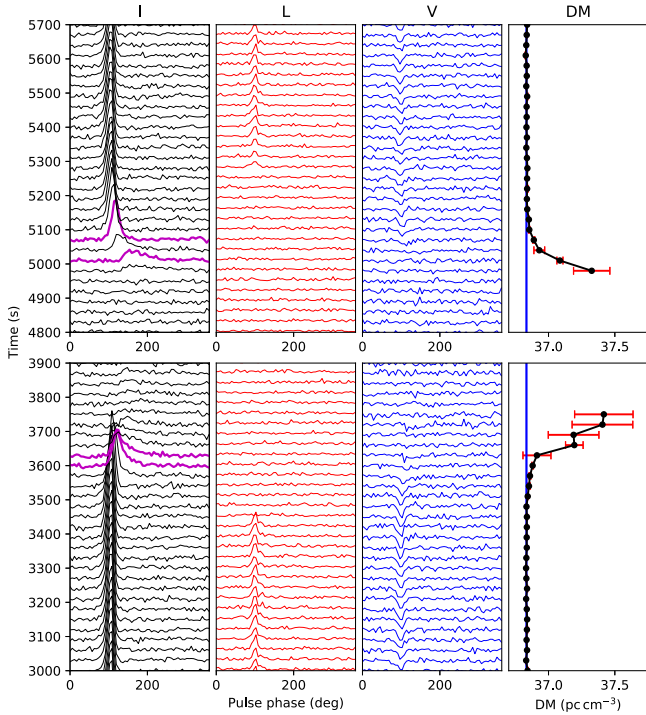


**Figure 4.** Total intensity, I (black), linear polarization, L (red), and circular polarization, V (blue), average pulse profiles of PSR J1720–0533 during the ingress (bottom panels) and egress (upper panels) of the eclipse. The magenta lines are the last and first pulses before and after the eclipse. The corresponding DM (black dots) variations of the eclipse are shown in the right panels. The red bars are the DM uncertainties. The horizontal blue line is for the DM of  $36.8337 \pm 0.0006 \text{ cm}^{-3} \text{ pc}$ , which is obtained by fitting the average out-of-eclipse profile.

variations are shown in the right panels of Figure 4. We also fitted the DM of the average out-of-eclipse profile and obtained a DM of  $36.8337 \pm 0.0006 \text{ cm}^{-3} \text{ pc}$ . As expected, the DM near the eclipse increases significantly and the maximum DM variations ( $\Delta\text{DM}$ ) during the ingress and egress of the eclipse are about  $0.6 \pm 0.2 \text{ cm}^{-3} \text{ pc}$  and  $0.5 \pm 0.1 \text{ cm}^{-3} \text{ pc}$ , respectively.

By analyzing the data with a subintegration of 30 s, the polarization profiles of the pulses near the eclipse of PSR J1720–0533 are shown in Figure 4. Note that the out-of-eclipse RM of  $21 \pm 1 \text{ rad m}^{-2}$  was used to correct the profiles. We found that the linear polarization disappears earlier than both the total and circular polarized profiles during the ingress and it appears later during the egress. The times when the linear polarization disappears and appears are 3450 s and 5250 s, respectively, but the profiles of the total intensities at these times do not show significant variations. The corresponding  $\Delta\text{DMs}$  are  $0.003 \pm 0.004 \text{ cm}^{-3} \text{ pc}$  and  $0.005 \pm 0.001 \text{ cm}^{-3} \text{ pc}$ , respectively, which does not show significant variations.

The pulse profiles near the eclipse become wider than that of the out-of-eclipse profile (the left panels of Figure 4). The dispersion smearing across each frequency channel is about  $19 \mu\text{s}$  for PSR J1720–0533, which can be negligible compared to the pulse profile. The scattering of the eclipse medium gives rise to an exponential decay of the pulse (Williamson 1972). We used the measured DM value to correct the profile, and then divided the entire band into four equal subbands with central frequencies of 1100 MHz, 1200 MHz, 1300 MHz, and 1400 MHz, respectively, and used a convolution of a Gaussian function with the exponential decay to fit the profile at each

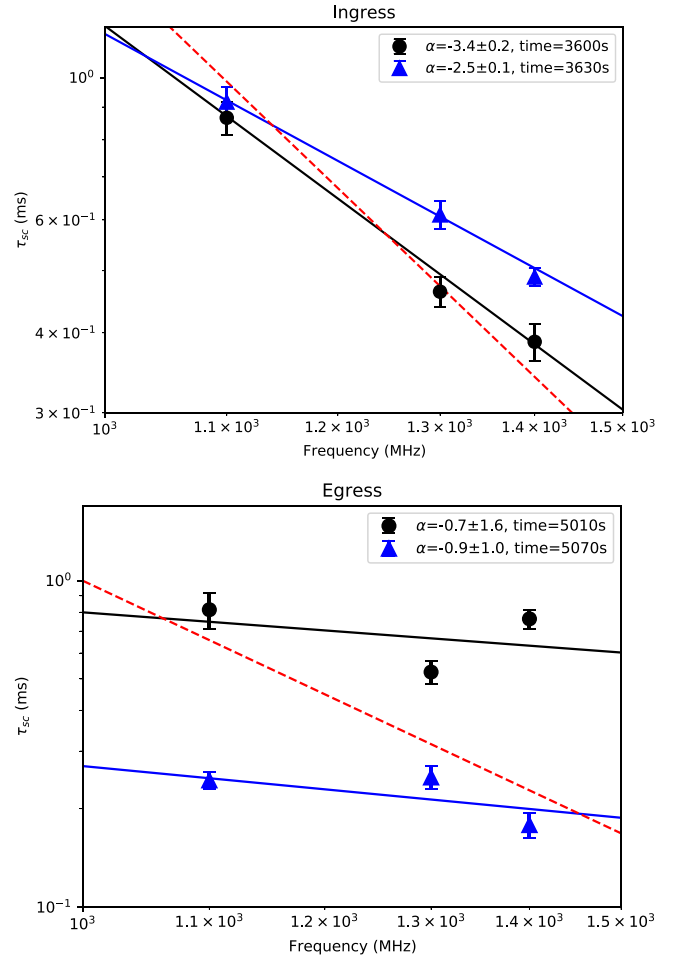


**Figure 5.** The scatter-broadening times  $\tau_{\text{sc}}$  at different frequencies for PSR J1720–0533. The solid lines are the power-law fittings with index  $\alpha$ , and the dashed lines show the thin-screen Kolmogorov prediction with index  $\alpha = -4.4$  (Lee & Jokipii 1976). Note that we did not fit the profiles at 1200 MHz because of the limited S/N.

band. We chose four bright profiles near the eclipse at the times of 3600 s, 3630 s, 5010 s, and 5070 s, respectively (the magenta lines in Figure 4). The  $\tau_{\text{sc}}$  variations with the frequency of these four profiles are shown in the upper and bottom panels of Figure 5, respectively; the solid lines show the the power-law fittings, and the dashed lines show the thin-screen Kolmogorov prediction with index  $\alpha = -4.4$  (Lee & Jokipii 1976). Note that we did not fit the profiles at 1200 MHz because of the limited signal-to-noise ratio (S/N). As seen, the scatter-broadening time becomes larger while the index becomes smaller during ingress. However, the index does not show significant variations during egress. Polzin et al. (2020) showed evidence for the presence of an eclipse mechanism that only smears out pulsations while it does not remove the flux for PSR J1816+4510, and attributed this to scattering in outflowing material from the companion. It is also a possible scenario for PSR J1720–0533. The scattering may also play an important role in the eclipse mechanism of PSR J1720–0533.

#### 4. Discussion and Conclusions

We present a high-sensitivity observation of newly discovered black widow pulsar PSR J1720–0533 using FAST. The scintillation maximum throughout the eclipse in our observation provides an opportunity to study the emission

variations near the eclipse in detail. We found there are quasi-periodic pulse intensity modulations with a period of  $\sim 22$  s during the ingress of the eclipse. No such emission modulations are detected during the egress of the eclipse. The eclipse is asymmetric, and the duration of ingress is longer than that of egress. The modulation during the ingress shows similar properties to the highly variable emissions throughout the eclipse of PSR J2051–0827, which are attributed to lensing by the intrabinary material (Lin et al. 2021). The phenomenon of PSR J2051–0827 demonstrates a link between DM and lensing. We suggested the plasma lensing possibly occurs in PSR J1720–0533 as well. Unfortunately, the DM variations of each modulation cluster during the ingress of PSR J1720–0533 cannot be measured precisely because of the limited S/N.

For PSR J2051–0827, the radiation beam sweeps across the edge of the eclipsed medium (Stappers et al. 2001) and the emissions do not completely disappear during the eclipse. The plasma lensing occurs throughout the entire eclipse, and the maximum  $\Delta\text{DM}$  during the eclipse is about  $0.07 \text{ cm}^{-3} \text{ pc}$  (Lin et al. 2021). However, for PSR J1720–0533, the emission is blocked by the eclipsed medium completely during the eclipse with a much longer eclipse duration, and the plasma lensing only occurs during the ingress of the eclipse. The maximum  $\Delta\text{DM}$  during the eclipse ingress is about  $0.6 \pm 0.2 \text{ cm}^{-3} \text{ pc}$ , which is similar to that during the egress of  $0.5 \pm 0.1 \text{ cm}^{-3} \text{ pc}$ . If the DM variations are tied to the flux density variations (Lin et al. 2021), the different DM variations during egress may account for the different timescale compared to ingress.

Besides PSR J1720–0533 and PSR J2051–0827, plasma lensing has been detected in two other spider pulsars: PSR B1744–24A (Bilous et al. 2019) and PSR B1957+20 (Main et al. 2018) with different manifestations. Unusually bright single pulses are detected largely near eclipse ingress and egress of the two pulsars, have intensities up to dozens of times that of the average pulse intensity, and have a pulse shape similar to that of the average pulse profile. It is difficult to explain these bright pulses via scintillation in the interstellar medium, as a separate emission mode, or as conventional giant pulses. The authors suggested these bright pulses are attributed to the lensing by the eclipsed medium (Main et al. 2018; Bilous et al. 2019). The duration of these bright pulses is approximately dozens of milliseconds, which is much shorter than that seen in PSR J1720–0533 and PSR J2051–0827 with a duration of dozens of seconds.

To estimate the size and location of the plasma lens, a single 1D lens model of Cordes et al. (2017) was used and the DM within the lens was assumed to follow Gaussian distribution. The size of the lens is  $a_{\text{lens}} = aR_{\text{sep}}$ , and the distance from the pulsar to the lens is  $d_{\text{sl}} = dR_{\text{sep}}$  with the separation between pulsar and companion  $R_{\text{sep}}$  and the dimensionless quantities  $a$  and  $d$ . The Fresnel scale at the lens plane is  $r_{\text{F}} \approx \sqrt{cd_{\text{sl}}d_{\text{lo}}/\nu d_{\text{so}}}$ , where  $\nu$  is the observation frequency,  $c$  is the velocity of light,  $d_{\text{lo}}$  and  $d_{\text{so}}$  are the distance from the observer to the lens and from the observer to the pulsar, respectively. We assume  $d_{\text{so}} \approx d_{\text{lo}}$  because the lens is much closer to the pulsar than to the observer. The maximum pulse amplification is  $G \sim a_{\text{lens}}/r_{\text{F}}$ . The time of caustic crossing  $t_{\text{c}} \sim a_{\text{lens}}(\delta G/G)/v_{\text{trans}}G^2 \cdot d_{\text{lo}}/d_{\text{so}}$  with the effective transverse velocity  $v_{\text{trans}}$ . We take  $v_{\text{trans}}$  as the orbital velocity of the companion,  $G = 1.6$ ,  $\delta G/G \approx 1$  and  $t_{\text{c}} \approx 20$  s, and obtained that  $a \approx 2.6 \times 10^{-2}$  and  $d \approx 9.8 \times 10^5$ . The corresponding lens size  $a_{\text{lens}} \approx 2.3 \times 10^4$  km.

The pulse emission of PSR J1720–0533 becomes depolarized near the eclipse, like PSR J1748–2446A (You et al. 2018) and PSR J2256–1024 (Crowter et al. 2020). The depolarization occurs when the RM shows rapid time variations (You et al. 2018). The fluctuations of the DM and/or parallel component of the magnetic field in the eclipse medium can result in rapid RM variations. For PSR J1720–0533, the DM variations at the orbital phases where the linear polarization disappears during the eclipse ingress and egress are  $0.003 \pm 0.004 \text{ cm}^{-3} \text{ pc}$  and  $0.005 \pm 0.001 \text{ cm}^{-3} \text{ pc}$ , respectively, which is almost unchanged. Therefore, the RM variations are more likely results from the fluctuations of the parallel component of the magnetic field in the eclipse medium and causes the depolarization of PSR J1720–0533. Our results suggest that there may be a significant magnetic field in the eclipse medium.

We then estimated the magnetic field strength of the eclipse medium. For spider pulsars, the pressure of the pulsar wind  $P_{\text{pw}} = \pi \dot{P}/ca^2P^3$  with the pulsar period  $P$ , the derivative of period  $\dot{P}$ , the pulsars inertia moment  $I$ , the orbital separation  $a$ , and the speed of light  $c$ . The magnetic pressure of the companion wind  $P_{\text{cw}} = B_{\text{E}}^2/8\pi$  with the magnetic field strength  $B_{\text{E}}$ . If the pulsar wind pressure equals the magnetic pressure of the companion wind at the interface,  $P_{\text{pw}} = P_{\text{cw}}$  (Thompson et al. 1994),  $B_{\text{E}} = 51P_{-3}^{-3/2}\dot{P}_{-20}^{1/2}a_{11}^{-1}$  taking  $I = 10^{45} \text{ g cm}^2$ , where  $a_{11}$  is the orbital separation in the units of  $10^{11} \text{ cm}$ ,  $P_{-3}$  and  $\dot{P}_{-20}$  are the spin period in the units of  $10^{-3} \text{ s}$ , and the time derivative of period in the units of  $10^{-20} \text{ s s}^{-1}$ . For PSR J1720–0533,  $P = 3.26 \text{ ms}$ ,  $\dot{P} = 7.46 \times 10^{-21} \text{ s s}^{-1}$ , and  $a = 1.3 R_{\odot}$ , the implied magnetic field of the eclipse medium  $B_{\text{E}} \approx 8 \text{ G}$ .

We also studied the effect of scattering near the eclipse of PSR J1720–0533. We found that the scatter-broadening time is frequency dependent during the ingress. Our results suggest that the scattering plays an important role in the eclipse at 1250 MHz for PSR J1720–0533. Our result is consistent with the conclusion of Thompson et al. (1994) that pulse smearing is more important for the eclipse at higher frequency for spider pulsars. Polzin et al. (2020) presented observations with the pulsed and imaged continuum fluxes simultaneously and found that the continuum flux of PSR J1816+4510 is consistent with the pulsed flux during ingress, but it extends to a significantly earlier orbital phase than the corresponding pulse flux in one egress of the eclipse. They suggested that this may result from scattering in outflowing material from the companion, and it seems that the scattering only occurs during the eclipse egress of PSR J1816+4510. For PSR J1720–0533, the scattering only occurs during the ingress in our observation; further observations with the pulsed and continuum fluxes simultaneously using FAST will provide more information on the eclipse.

This work is supported by the the National SKA Program of China (No. 2020SKA0120100), National Natural Science Foundation of China (No. 12041304, No. 12041303, No. 12163001, No. U1938117, and No. U1731238), the National Key Research and Development Program of China (No. 2017YFA0402600), the Youth Innovation Promotion Association of Chinese Academy of Sciences, the 201\* Project of Xinjiang Uygur Autonomous Region of China for Flexibly Fetching in Upscale Talents, China Postdoctoral Science Foundation (No. 2020M681758), the Operation, Maintenance and Upgrading Fund for Astronomical Telescopes and Facility Instruments, budgeted from the Ministry of Finance of China

(MOF) and administrated by the Chinese Academy of Science (CAS), the Key Lab of FAST, National Astronomical Observatories, Chinese Academy of Sciences, and the Guizhou Provincial Science and Technology Foundation (No. [2020] 1Y016). This work made use of the data from the Five-hundred-meter Aperture Spherical radio Telescope, which is a Chinese national mega-science facility, operated by National Astronomical Observatories, Chinese Academy of Sciences. The authors wish to thank K. Liu and F.X. Lin for useful suggestions and comments that improved the manuscript.

*Software:* DSPSR (van Straten & Bailes 2011), PSRCRIVE (Hotan et al. 2004), TEMPO2 (Hobbs et al. 2006).

### ORCID iDs

S. Q. Wang  <https://orcid.org/0000-0003-4498-6070>

### References

- Alpar, M. A., Cheng, A. F., Ruderman, M. A., & Shaham, J. 1982, *Natur*, 300, 728
- Archibald, A. M., Stairs, I. H., Ransom, S. M., et al. 2009, *Sci*, 324, 1411
- Bhattacharya, D., & van den Heuvel, E. P. J. 1991, *PhR*, 203, 1
- Bilous, A. V., Ransom, S. M., & Demorest, P. 2019, *ApJ*, 877, 125
- Cordes, J. M., Wasserman, I., Hessels, J. W. T., et al. 2017, *ApJ*, 842, 35
- Crowter, K., Stairs, I. H., McPhee, C. A., et al. 2020, *MNRAS*, 495, 3052
- Deneva, J. S., Ray, P. S., Camilo, F., et al. 2016, *ApJ*, 823, 105
- Fruchter, A. S., Stinebring, D. R., & Taylor, J. H. 1988, *Natur*, 333, 237
- Hobbs, G. B., Edwards, R. T., & Manchester, R. N. 2006, *MNRAS*, 369, 655
- Hotan, A. W., van Straten, W., & Manchester, R. N. 2004, *PASA*, 21, 302
- Jiang, P., Yue, Y., Gan, H., et al. 2019, *SCPMA*, 62, 959502
- Lee, L. C., & Jokiipii, J. R. 1976, *ApJ*, 206, 735
- Li, D., Wang, P., Qian, L., et al. 2018, *IMMag*, 19, 112
- Lin, F. X., Main, R. A., Verbiest, J. P. W., Kramer, M., & Shaifullah, G. 2021, *MNRAS*, 506, 2824
- Main, R., Yang, I. S., Chan, V., et al. 2018, *Natur*, 557, 522
- Patruno, A., Haskell, B., & Andersson, N. 2017, *ApJ*, 850, 106
- Polzin, E. J., Breton, R. P., Bhattacharyya, B., et al. 2020, *MNRAS*, 494, 2948
- Polzin, E. J., Breton, R. P., Clarke, A. O., et al. 2018, *MNRAS*, 476, 1968
- Polzin, E. J., Breton, R. P., Stappers, B. W., et al. 2019, *MNRAS*, 490, 889
- Roberts, M. S. E. 2013, in Proc. of the IAU 291, ed. J. van Leeuwen (Cambridge: Cambridge Univ. Press), 127
- Stappers, B. W., Archibald, A. M., Hessels, J. W. T., et al. 2014, *ApJ*, 790, 39
- Stappers, B. W., Bailes, M., Lyne, A. G., et al. 2001, *MNRAS*, 321, 576
- Tavani, M., & Brookshaw, L. 1991, *ApJL*, 381, L21
- Thompson, C., Blandford, R. D., Evans, C. R., & Phinney, E. S. 1994, *ApJ*, 422, 304
- van Straten, W., & Bailes, M. 2011, *PASA*, 28, 1
- Williamson, I. P. 1972, *MNRAS*, 157, 55
- Yao, J. M., Manchester, R. N., & Wang, N. 2017, *ApJ*, 835, 29
- You, X. P., Manchester, R. N., Coles, W. A., Hobbs, G. B., & Shannon, R. 2018, *ApJ*, 867, 22